







Absence of zero-field-cooled exchange bias effect in single crystalline $\text{La}_{2-x}\text{A}_x\text{CoMnO}_6$ ($A = \text{Ca}, \text{Sr}$) compounds

C. Macchiutti ¹, J. R. Jesus,¹ F. B. Carneiro ¹, L. Bufaiçal ², M. Ciomaga Hatnean ³, G. Balakrishnan ³, and E. M. Bittar ^{1,*}

¹Centro Brasileiro de Pesquisas Físicas, Rio de Janeiro, Rio de Janeiro 22290-180, Brazil

²Instituto de Física, Universidade Federal de Goiás, Goiânia 74001-970, Brazil

³Department of Physics, University of Warwick, Coventry CV4 7AL, United Kingdom



(Received 25 May 2021; accepted 26 August 2021; published 7 September 2021)

Magnetic properties of $A_2BB'O_6$ ($A = \text{rare or alkaline-earth ions}$; $B, B' = \text{transition-metal ions}$) double perovskites are of great interest due to their potential spintronic applications. Particularly fascinating is the zero-field-cooled exchange bias effect observed for the hole-doped $\text{La}_{2-x}\text{A}_x\text{CoMnO}_6$ polycrystalline samples. In this paper we synthesize $\text{La}_2\text{CoMnO}_6$, $\text{La}_{1.5}\text{Ca}_{0.5}\text{CoMnO}_6$, and $\text{La}_{1.5}\text{Sr}_{0.5}\text{CoMnO}_6$ single crystals by the floating zone method and study their magnetic behavior. The three materials are ferromagnetic. Surprisingly, we observe no zero or even conventional exchange bias effect for the Ca- and Sr-doped single crystals, in sharp contrast to polycrystalline samples. This absence indicates that the lack of grain boundaries and spin-glass-like behavior, not observed in our samples, might be key ingredients for the spontaneous exchange bias phenomena seen in polycrystalline samples.

DOI: [10.1103/PhysRevMaterials.5.094402](https://doi.org/10.1103/PhysRevMaterials.5.094402)

I. INTRODUCTION

Materials displaying general formula $A_2BB'O_6$ ($A = \text{rare or alkaline-earth ions}$; $B, B' = \text{transition-metal ions}$) and double perovskite structure present intriguing physical phenomena due to the interplay among structural, magnetic, and electrical properties [1]. There is great interest in this family of compounds due to the possible applications in spintronic devices. Particularly interesting is the zero-field-cooled (ZFC) exchange bias (ZEB) effect recently observed for hole-doped members of this family of compounds [2–9]. The conventional exchange bias (CEB) effect is characterized as a shift in hysteresis loop measurements, observed after cooling the system in the presence of an external magnetic field [10]. In materials in which the ZEB effect is seen, the shift in magnetization as a function of the applied field is detected spontaneously in zero-field cooling [2–9]. In these double perovskites, the ZEB effect may result from a reentrant spin-glass-like phase in which magnetic relaxation of unusual glassy moments affects the magnetization loop shifts [11,12].

The intrinsic magnetic inhomogeneity caused by different transition-metal ions in double perovskites commonly leads to spin-glass-like behavior, making these materials good candidates to understand the mechanisms ruling the ZEB effect. The crystal structure of $A_2BB'O_6$ double perovskites is significantly influenced by the A , B , and B' cations and their ionic radii size mismatch. One can describe this mismatch by the Goldschmidt tolerance factor t , where $t = (r_A + r_O)/\sqrt{2}(\langle r_B \rangle + r_O)$, r_A , $\langle r_B \rangle$, and r_O are the ionic radii of A and the average of B/B' and O, respectively [13].

The ideal tolerance factor is given by $t = 1$, which denotes the cubic rock-salt ordered and space-group $Fm-3m$ structure. Although $t < 1$ indicates that the A cation ionic radii are smaller than ideal, and the structure compensates for its size mismatch by tilting the $BO_6/B'O_6$ octahedra. By decreasing slightly the tolerance factor the structure typically evolves to lower crystal symmetries as $Fm-3m \rightarrow I4/m \rightarrow R-3 \rightarrow I2/m \rightarrow P2_1/n$ [1]. For ordered structures, a perfect sequence of $B-O-B'$ chains are formed, whereas when the disorder is present, a random distribution of B and B' cations in which $B-O-B$, $B-O-B'$, and $B'-O-B'$ chains can occur. In disordered double perovskites, the ideal structure is the $Pm-3m$ space group, whereas the most common is $Pnma$ [1].

The $\text{La}_{2-x}\text{A}_x\text{CoMnO}_6$ ($A = \text{Ca}, \text{Sr}$; $x = 0, 0.5$) family of compounds have been studied over many years. The parent $\text{La}_2\text{CoMnO}_6$ (LCMO) material is known to show ferromagnetic behavior due to superexchange $\text{Co}^{2+}\text{-O-Mn}^{4+}$ coupling, according to Goodenough-Kanamori-Anderson (GKA) rules [14,15] with potential multiferroic properties [16,17]. The Curie temperature (T_C) for ordered samples can reach up to 226 K [18] with a saturation spin moment $M_{\text{sat}} = 6 \mu\text{B/f.u.}$, whereas the disordered ones, e.g., with oxygen deficiency and/or antisite defects, present lower T_C and M_{sat} [2,18,19]. If changes in the B -cation valence also occur, a $\text{Co}^{3+}\text{-O-Mn}^{3+}$ ferromagnetic interaction may happen, and a distinct ferromagnetic transition is present [5,14,17,18]. Also, the disorder can generate antiferromagnetic clusters, giving rise to an antiferromagnetic transition temperature T_N because of exchange $\text{Co}^{3+}\text{-O-Mn}^{4+}$ coupling and/or antiphase boundaries of $\text{Co}^{2+}\text{-Co}^{2+}$ or $\text{Mn}^{4+}\text{-Mn}^{4+}$ pairs [14,20]. Regarding its crystal structure, LCMO is mostly described as a monoclinic $P2_1/n$ space group for an ordered population of the B sites and orthorhombic $Pnma$ when the disorder is present [5,18].

*bittar@cbpf.br

For $\text{La}_{1.5}\text{Ca}_{0.5}\text{CoMnO}_6$ (LCCMO) and $\text{La}_{1.5}\text{Sr}_{0.5}\text{CoMnO}_6$ (LSCMO) materials, it has been reported in polycrystalline samples that by substituting the La^{3+} cation by 25% of an alkaline-earth ion with 2+ valence, gives rise to a spin-glass phase which promotes the unusual ZEB effect [2,3,5,7,11,12]. It was also shown that Ba doping can tune the ZEB effect in LSCMO [21]. In polycrystalline LCCMO, a phase segregation with a mixture of two $Pnma$ space groups in 94% and 6% concentrations was seen, whereas LSCMO showed 91% of rhombohedral $R3c$ and 9% of $Pnma$ phases [5]. Magnetic properties of both samples showed two ferromagnetic (T_C) and one antiferromagnetic (T_N) transition temperatures, $T_{C1} \sim 158$, $T_{C2} \sim 141$, and $T_N \sim 62$ K for LCCMO; and $T_{C1} \sim 180$, $T_{C2} \sim 157$, and $T_N \sim 74$ K for LSCMO. Both polycrystalline compounds exhibit the onset of cluster glass behavior at lower temperatures due to the presence of competing magnetic phases [5].

Since the CEB is an interface effect [10], it is usually observed in polycrystalline core-shell systems or heterostructured thin films presenting two or more magnetic phases. Similarly, for the ZEB effect, most studies in the literature have focused on polycrystalline materials. In single crystals, however, the reports of the ZEB phenomenon are scarce. There is an intersection between different single crystalline perovskite compounds, such as $\text{La}_{0.82}\text{Sr}_{0.18}\text{CoO}_3$ [22], $\text{Y}_{0.95}\text{Eu}_{0.05}\text{MnO}_3$ [23], and SmFeO_3 [24–26], that show an essential role of a spin-glass phase for the observance of the ZEB effect in these materials. Thus, additional research in similar systems is desired to understand the phenomenon thoroughly.

Here we present our paper on single crystalline double perovskite LCMO, LCCMO, and LSCMO compounds where we investigate their structural and magnetic properties, comparing their characteristics with the polycrystals. All samples are ferromagnetic below T_C with a clear indication of two ferromagnetic transitions for LCMO and LCCMO. Changes in T_C between these oxides are accounted for by structural modifications of the $B\text{-O-B}$ bond angle, $B\text{-O}$ bond length, and crystallinity. We observe no glassy-like phase for the three materials and the absence of the ZEB effect for LCCMO and LSCMO. Therefore, the nonexistence of grain boundaries and spin-glass-like behavior indicate that these are critical ingredients for the spontaneous exchange bias phenomena seen in polycrystalline samples.

II. EXPERIMENTAL DETAILS

Polycrystalline powders of LCMO, LCCMO, and LSCMO materials were synthesized via the solid-state reaction, details of the process have been reported elsewhere [5]. The crystal growths were carried out by the floating zone technique using two different two-mirror image furnaces (NEC SC1MDH-11020 Canon Machinery, Inc. and Quantum Design IR Image Furnace) in air. The feed rods needed for the crystal growths were hydrostatically pressed up to 50 MPa into the form of cylindrical rods and sintered in air at 1300 °C for 12 h (LCMO), 1300 °C for 24 h (LCCMO), and 1400 °C for 24 h (LSCMO). Crystals were grown at a rate of 3–5 mm/h with the feed and seed rods, each rotating at 20 rpm in opposite directions. The structural properties of the samples

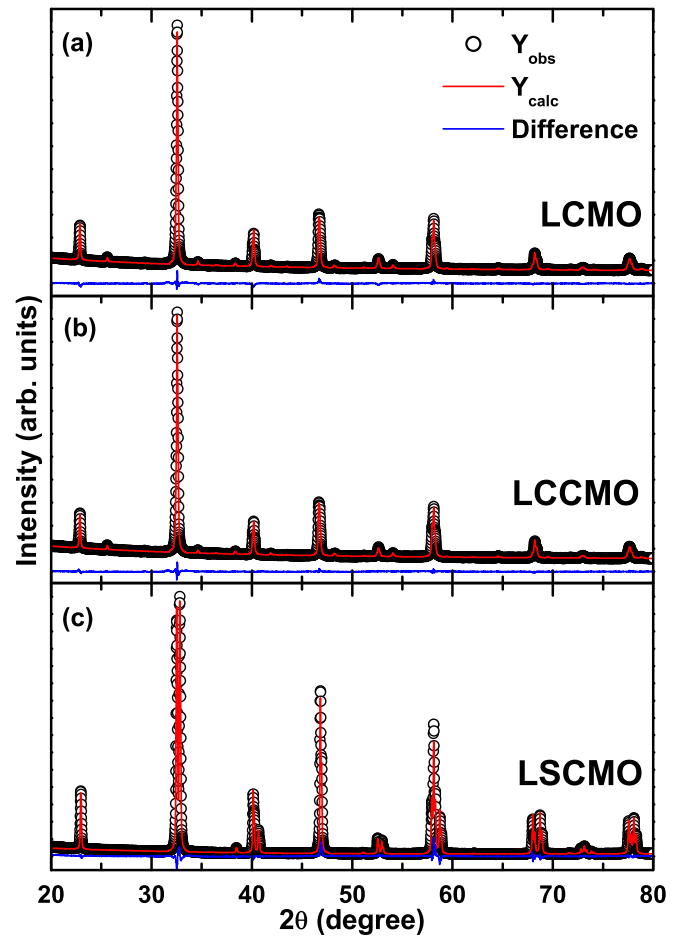


FIG. 1. Conventional $\text{Cu } K_{\alpha}$ x-ray powder-diffraction patterns for (a) LCMO, (b) LCCMO, and (c) LSCMO. Open black circles are experimental data; red curves calculated Rietveld refinement; blue curves are the difference between the observed and the calculated patterns.

were investigated by conventional x-ray powder diffraction (XRPD) measurements using a PANalytical Empyrean diffractometer with $\text{Cu } K_{\alpha}$ radiation ($\lambda = 1.5406 \text{ \AA}$). All data were collected in Bragg-Brentano geometry in the continuous mode with the 2θ range from 20° to 80° , step size of 0.013° , and a scanning speed of $0.5^{\circ}/\text{min}$. Rietveld refinements were performed using the GSAS+EXPGUI suite [27]. X-ray Laue backscattering patterns were recorded using a commercial Photonic Science Laue System for cutting and aligning the samples along different directions for magnetic measurements. Roughly, 5-mm size single crystals were extracted from the crystal boules. Magnetic and thermal properties characterization were carried out using Quantum Design physical property measurement system equipment.

III. RESULTS

A. Structural characterization

Figure 1 shows the XRPD patterns collected on LCMO, LCCMO, and LSCMO samples. These powdered samples were obtained by powdering a small section of the as-grown boule and measured at room temperature. For the three

TABLE I. Main results obtained from the Rietveld refinements of the XRPD data.

	LCMO	LCCMO	LSCMO
Space group	<i>Pnma</i>	<i>Pnma</i>	<i>R-3c</i>
<i>a</i> (Å)	5.4699(3)	5.4908(1)	5.5130(1)
<i>b</i> (Å)	7.7182(3)	7.7668(1)	5.5130(1)
<i>c</i> (Å)	5.4607(2)	5.5121(1)	13.3183(1)
$\langle B-O \rangle$ (Å)	1.9520(12)	1.9806(1)	1.9581(3)
$\langle B-O-B \rangle$ (°)	162.6(11)	159.2(4)	164.5(1)
R_p (%)	3.8	1.2	3.5
R_{wp} (%)	5.7	1.8	4.7

samples all the Bragg peaks could be indexed using the double perovskite structure model, and no impurity peaks could be observed. The crystal structure was indexed with orthorhombic symmetry and space-group *Pnma* for the LCMO and LCCMO; whereas LSCMO is rhombohedral space-group *R-3c*. Lattice parameters (see Table I) are in good agreement with the data reported for polycrystalline samples in literature [5]. Figure 2 shows the x-ray Laue backscattering patterns of the three LCMO, LCCMO, and LSCMO samples after the as-grown single crystal boules [Fig. 2(d)] were oriented and cut along the [001] crystalline direction. Figure 2(b) presents better-defined diffraction spots resulting from a more homogeneous sample. It indicates that the proximity between La³⁺ and Ca²⁺ ionic radii leads to a better accommodation of these ions in the LCCMO structure than LSCMO resulting from the incorporation of large Sr²⁺ ions. The LCCMO has less residual stress and better crystal quality manifested in the goodness of fit parameters obtained from the Rietveld refinements (see Table I).

B. Magnetic properties

The ZFC and field-cooled (FC) temperature-dependent magnetization of the LCMO, LCCMO, and LSCMO materials are shown in Fig. 3 under an applied magnetic-field (*H*) of 0.1 kOe along the [001] direction. No appreciable qualitative changes were observed for *H* ⊥ [001] for all samples (not shown). The magnetic irreversibility of the ZFC and FC

curves observed at the paramagnetic to ferromagnetic transition for LCMO, LCCMO, and LSCMO is usually ascribed to a glassylike magnetic behavior. Especially for LCMO and LCCMO, the ZFC magnetization only starts to grow at around *T* = 75 K.

In order to investigate this hypothesis, were performed measurements of the *ac* susceptibility in-phase component (χ') as a function of temperature as shown in Fig. 4. Although some changes in the intensities of the *ac* curves could be noted on the low-temperature side of the peaks carried at different frequencies, no systematic variations in the temperature of the peaks were observed, indicating no canonical glassy phase nor relevant dynamic effects [28]. Conversely, this indicates that such frequency dependence of the *ac* intensity is most likely related to the onset of a second ferromagnetic transition extended over a broad temperature range as will be discussed in the next section. The magnetic irreversibility observed can be attributed to the domain-wall motion depinning process as previously seen in other double perovskite single crystals [29,30]. Table II summarizes the magnetic ordering transition temperatures for all studied materials. We could not obtain the effective moment nor the Curie-Weiss temperature due to limitations of the maximum temperature measured (*T* = 400 K), preventing a good linear fit in the paramagnetic region.

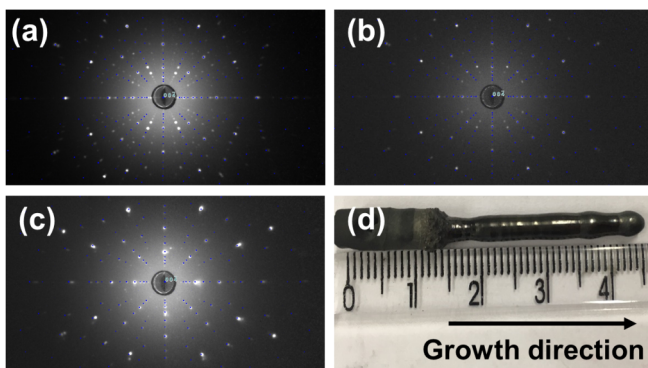


FIG. 2. X-ray Laue backreflection photograph, showing the [001] orientation of an aligned sample piece used for physical property measurements for (a) LCMO, (b) LCCMO, and (c) LSCMO. (d) LCCMO as-grown single crystal boule grown by the floating zone method.

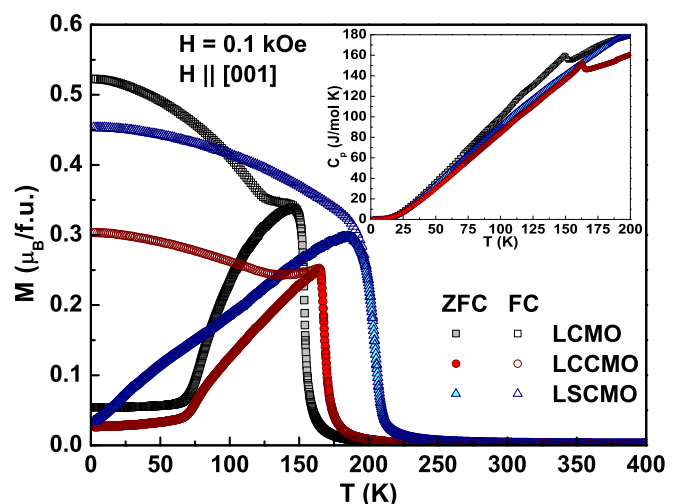


FIG. 3. LCMO, LCCMO, and LSCMO as-grown single crystals temperature dependence of the ZFC and FC magnetization curves for *H* || [001], measured at *H* = 0.1 kOe. The inset: Zero-magnetic-field heat capacity as a function of temperature.

TABLE II. Main results obtained from the temperature dependence of the magnetization and ZFC $M(H)$ curves.

Sample	LCMO	LCCMO	LSCMO
T_C (K)	150(1)	165(2)	205(2)
T'_C (K)	116(2)	120(2)	
H_C (Oe)	1396(116)	626(112)	1380(88)
M_S (μ_B /f.u.)	6.3(1)	6.8(1)	6.5(1)
M_R (μ_B /f.u.)	2.4(1)	0.7(1)	2.7(1)

Nevertheless, this is an indication of short-range magnetic correlations even at temperatures well above the ordering temperatures. Figure 5 shows the magnetization hysteresis loop at $T = 5$ K and up to $H = 90$ kOe for LCMO, LCCMO, and LSCMO. These curves were obtained after zero-field cooling the samples. A sharp ferromagneticlike hysteresis is seen for all three samples, and the magnetization saturates at $M_S \sim 6\mu_B$ /f.u. for $H > 40$ kOe. We see no hysteresis loop shifts, i.e., no ZEB effect for LCCMO and LSCMO single crystals (see the right side inset of Fig. 5), in contrast to what was observed in polycrystals [2–5,7,9]. Also, we do not observe the conventional EB effect after FC at $H = 9$ T for all samples (not shown). In addition, no appreciable changes for the magnetization hysteresis loop either at ZFC or at FC at $H = 9$ T for the other orthogonal crystalline directions were

seen (not shown). A metamagnetic transition can be noted for LCCMO (see the left side inset of Fig. 5).

IV. DISCUSSION

A. LCMO

Regarding the magnetic properties for LCMO, we observe two ferromagnetic transitions, a majority ferromagnetic phase at $T_C \sim 150(1)$ K and a minority ferromagnetic phase at $T'_C \sim 116(2)$ K as seen from the FC curve in Fig. 3. T_C is similar as reported before for single crystals [29,31]. These magnetic phase transitions are supported by the zero-magnetic-field heat-capacity measurement, showing one broad peak at approximately 116 K and another sharper at around 150 K (see the inset of Fig. 3). In polycrystals it was seen by x-ray absorption spectroscopy measurements the presence of mixed valence Co ($\text{Co}^{2+}/\text{Co}^{3+}$) and Mn ($\text{Mn}^{3+}/\text{Mn}^{4+}$) [5,32]. Thus, by the GKA rules [14], one can ascribe these ferromagnetic orderings as the result of $\text{Co}^{2+}\text{-O-Mn}^{4+}$ (T_C) and $\text{Co}^{3+}\text{-O-Mn}^{3+}$ (T'_C) superexchange interactions with $T_C > T'_C$ [5,18,32]. The presence of Co^{3+} and Mn^{3+} was already reported for LCMO solution grown single crystals [31]. The ac susceptibility (Fig. 4) shows a frequency-independent peak within the experimental resolution approximately at 150 K. However, no peak is observed at around 116 K. This indicates

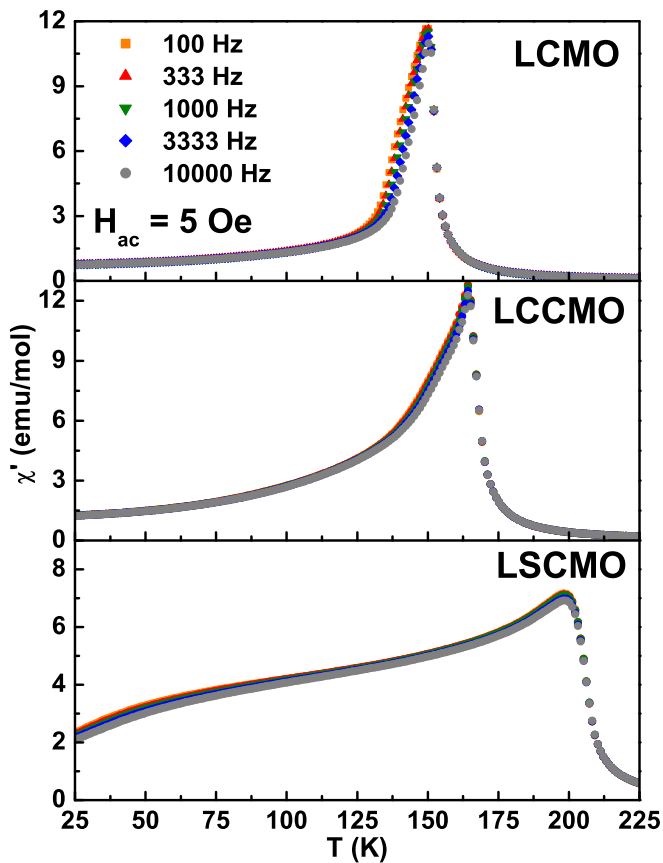


FIG. 4. LCMO, LCCMO, and LSCMO single crystals in-phase component of ZFC ac susceptibility (χ') as a function of temperature for different frequencies in a probing ac magnetic field of 5 Oe.

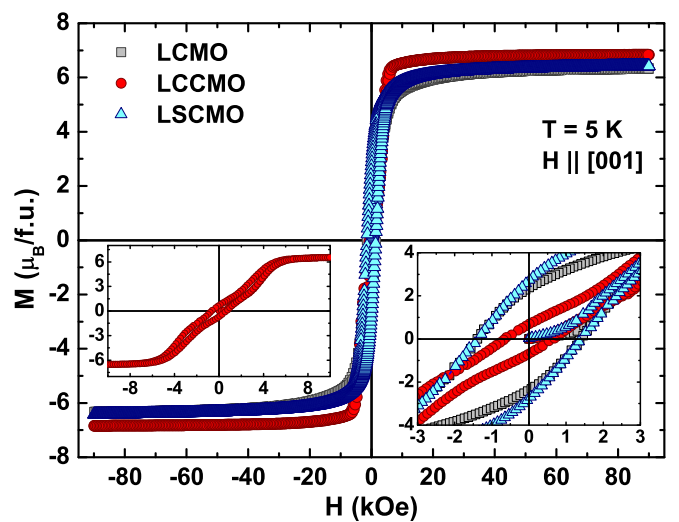


FIG. 5. LCMO, LCCMO, and LSCMO ZFC as-grown single crystals $M(H)$ curves for $H \parallel [001]$, measured at $T = 5$ K and $H_{\max} = 90$ kOe. The right inset shows the magnified view of the curves close to the $M = 0$ region. The left inset shows the LCCMO $M(H)$ curve.

that at T_C a long-range magnetic order sets in, whereas at T'_C the Co^{3+} -O- Mn^{3+} exchange interaction has more of a short-range character. The small frequency dependence for $125 < T < 150$ K indicates slow spin dynamics, which is not characteristic of a canonical glassy behavior and may be due to domain-wall motion.

Figure 5 shows a sharp ferromagnetic magnetization hysteresis loop (up to $H = 90$ kOe) which saturates at $M_S = 6.3(1) \mu_B/\text{f.u.}$ and has remanent magnetization $M_R = 2.4(1) \mu_B/\text{f.u.}$ (see Table II). For the fully ordered LCMO one would expect only the Co^{2+} -O- Mn^{4+} exchange interaction and $M_S = 6 \mu_B/\text{f.u.}$, consistent with the sum of Co^{2+} ($3d^7$, $S = 3/2$) and Mn^{4+} ($3d^3$, $S = 3/2$) states per formula unit [18]. Since the temperature dependence of magnetization of our single crystalline sample already gave us an indication of mixed valence, we must take into account Co^{3+} and Mn^{3+} spins to the saturated experimental value. Considering, high-spin Co^{3+} ($3d^6$, $S = 2$), and Mn^{3+} ($3d^4$, $S = 2$), one can estimate the amount of Co^{2+} -O- Mn^{4+} and Co^{3+} -O- Mn^{3+} couplings by equating the expression $M_S = 6.3 = [(1-x)(\text{Co}^{2+} + \text{Mn}^{4+}) + x(\text{Co}^{3+} + \text{Mn}^{3+})]$, thus, deriving that our LCMO sample has 15% of Co^{3+} -O- Mn^{3+} and 85% of Co^{2+} -O- Mn^{4+} interactions. In this rough approximation, we are neglecting the cationic disorder-induced contributions of antiferromagnetic couplings, such as Mn^{4+} - Mn^{4+} , Co^{2+} - Mn^{3+} , and Co^{2+} - Co^{2+} . And ferromagnetic couplings, for example, Mn^{3+} - Mn^{4+} . This consideration is a good approximation once $H = 90$ kOe may be sufficient to flip the great majority of the antiferromagnetic spins pointing toward the opposite direction to the external magnetic field.

B. LCCMO

By hole doping Ca^{2+} and Sr^{2+} into the La^{3+} site in the LCMO structure, one destabilizes the electron count, and in order to maintain charge neutrality, it is more likely that either some Mn^{3+} becomes Mn^{4+} or Co^{2+} transforms to Co^{3+} . Previous x-ray absorption spectroscopy measurements showed indications of a preference for the increase in the amount of Co^{3+} by alkaline-earth cations substitution in polycrystalline LCMO. At the same time, Mn is maintaining its mean valence value [5].

For LCCMO we observe a clear ferromagnetic transition at $T_C \sim 165(2)$ K (Figs. 3 and 4), slightly greater than for LCMO. It is also noted a broader second transition at $T'_C \sim 120$ K. The $M_S = 6.8(1) \mu_B/\text{f.u.}$ seen in Fig. 5 is also greater for LCCMO than for LCMO. Both results are due to the doping-induced electronic changes. Assuming that the Mn mean valence does not change with Ca doping, there should be an increase of 50% of Co^{3+} with respect to LCMO. One can calculate the expected saturation magnetization by the expression $M_S = [0.85\text{Mn}^{4+} + 0.15\text{Mn}^{3+} + (0.85 - 0.50)\text{Co}^{2+} + (0.15 + 0.50)\text{Co}^{3+}]$, which gives $M_S = 6.8 \mu_B/\text{f.u.}$, exactly the obtained experimental value. The increased disorder caused by changes in the valence of the transition-metal ions prevents the percolation of the Co^{3+} -O- Mn^{3+} coupling. This transition might be smeared over a wide temperature range (see the inset in Fig. 3)

as seen for the frequency dependence of χ' at $125 < T < 150$ K (Fig. 4).

The left inset of Fig. 5 highlights a steplike character in the $M(H)$ curve of LCCMO at $T \sim 5$ K. Such behavior was reported for similar compounds in which different mechanisms were said to explain such an effect. For $\text{Tb}_2\text{CoMnO}_6$ and $\text{Eu}_2\text{CoMnO}_6$ this steplike behavior was initially explained in terms of a field-induced metamagnetic transition from ferrimagnetism to ferromagnetism in the Co^{2+} -O- Mn^{4+} coupling [33]. Nevertheless, later on a more recent detailed investigation employing neutron powder diffraction ruled out such a possibility [34]. In this paper, the metamagnetic transition was explained in terms of the presence of a spin-glass-like phase and of the magnetic ordering of rare-earth ions in a direction distinct to those of Co and Mn [34,35]. In our case, in contrast to these hypotheses, the A-site ions are diamagnetic, and no sign of a spin-glass-like phase is observed. Thus, the characteristic feature observed in the $M(H)$ curve of LCCMO may be justified in terms of the two distinct ferromagnetic coupling contributions for the total magnetization.

C. LSCMO

The LSCMO sample present $T_C \sim 205(2)$ K (Table II) and a second ferromagnetic/antiferromagnetic transition at lower temperatures is not clear, in contrast to polycrystals [3,5]. As in LCCMO, one would expect an increase in the Co valence, although, for LSCMO, the saturated magnetization is slightly smaller [$M_S = 6.5(1) \mu_B/\text{f.u.}$], indicating that not only Co, but also Mn valence changes. If we assume that in LSCMO, all 15% of Mn^{3+} becomes Mn^{4+} , then only 35% of Co^{2+} shifts into Co^{3+} . Thus, the equation $M_S = [(0.85 + 0.15)\text{Mn}^{4+} + (0.15 - 0.15)\text{Mn}^{3+} + (0.85 - 0.35)\text{Co}^{2+} + (0.15 + 0.35)\text{Co}^{3+}] = 6.5 \mu_B/\text{f.u.}$, has the same value that the experimental magnetization saturates (Fig. 5). However, the weak frequency dependence in the in-phase component of the ac susceptibility at low temperatures indicates an almost negligible amount of Mn^{3+} may be present. In such a case, the diluted Co^{3+} - Mn^{3+} interaction would be then pushed to lower temperatures with respect to LCMO and LCCMO (Fig. 4).

The ferromagnetic transition temperature T_C increases for doped LCCMO and LSCMO regarding the undoped LCMO. Possible explanations to this, which might be counterintuitive, once doping causes disorder and also significantly promotes some Co^{2+} to Co^{3+} , may come from the crystal structure properties of these $A_2BB'O_6$ materials. The effect of the transition-metal exchange interaction (B -O- B) orbital overlapping geometry is more critical to strengthen T_C than disorder is to weaken it [20]. Therefore, one suitable structural parameter for this analysis is the B -O- B bond angle and the B -O bond length. The closer the bond angle is to 180° and the shorter the bond length is, the higher T_C is.

D. Conclusions

Considering the ionic radii of the following elements as being equal to La^{3+} (1.36 Å), Ca^{2+} (1.34 Å), Sr^{2+} (1.44 Å) [XII coordination]; Co^{2+} (0.745 Å), Co^{3+} (0.61 Å), Mn^{3+} (0.645 Å), Mn^{4+} (0.53 Å) [VI

coordination]; and O^{2-} (1.35 Å) [II coordination] [36], one can calculate the tolerance factor for each material as defined in the Introduction. The stable perovskite structure is guaranteed by $0.89 < t < 1.02$, and as t decreases, the crystalline lattice becomes rhombohedral ($0.96 < t < 1$) and orthorhombic ($t < 0.96$) [37]. As in previous polycrystalline samples [5], the parent LCMO compound has orthorhombic symmetry. The calculated tolerance factor for this material is $t \sim 0.96$, in agreement with the observed $Pnma$ space group. For LCCMO, we see a decrease in the bond angle and an increase in the bond length (see Table I). The calculated $t \sim 0.98$ indicates a preference for a rhombohedral atomic arrangement, although experimentally, we find the orthorhombic structure. However, the greater structural distortion due to doping gives rise to the tilting of the oxygen octahedra and accommodates the ions better in the crystal lattice, explaining the higher crystal homogeneity of the LCCMO sample when compared to LCMO and LSCMO [see Figs. 1(a) and 2(b) for sharper diffraction peaks and spots, respectively]. This higher degree of crystallinity could describe the small increase in T_C , despite the reduced bond angle and elongated bond length regarding LCMO. The calculated $t \sim 0.99$ for LSCMO produces a more symmetric rhombohedral crystal structure, and the bond angle is closer to 180° giving rise to the highest T_C .

Despite many works on the ZEB effect in polycrystalline Ca^{2+} - and Sr^{2+} -doped LCMO, our single crystals showed no signatures of such an effect (the right inset of Fig. 5). Neither did we observe the conventional magnetization as a function of applied field shift by cooling the materials under an external magnetic field ($H = 9$ -T cooling field; not shown). One key difference between poly and single crystals is the lack of grain boundaries in the latter in which the number of interfaces is drastically reduced. It is well established that the exchange bias effect is an interface phenomenon between different magnetic phases, usually a ferromagnetic/antiferromagnetic uncompensated moment interface [10]. Thus, in a single magnetic phase single crystal, it is expected that no conventional exchange bias effect is to be observed. The presence of a reentrant magnetic glassylike phase would, however, change this scenario. The slow dynamics of the spin-glass-like moments relaxation under a magnetic field would create an artificial interface of pinned moments, giving rise to the asymmetry in

the hysteresis loops [5,38–40]. In our LCCMO and LSCMO samples, we see no such glassylike phase. Therefore, the absence of the ZEB effect in single crystals attests to the need for a glassy magnetic phase for its insurgence in these types of materials [11,12]. In addition, we see some probable correlation of the ZEB effect magnitude with the grain boundary size in polycrystals, and further studies should verify this.

V. SUMMARY

Here we present our paper on the magnetic properties of single crystalline $La_{2-x}A_xCoMnO_6$ ($A = Ca, Sr; x = 0, 0.5$) materials. The crystalline structure of the single crystals is the same as found for polycrystalline samples [5], orthorhombic for LCMO and LCCMO, and rhombohedral for LSCMO. LCMO and LCCMO present two magnetic transitions ascribed to the Co^{2+} -O-Mn⁴⁺ and Co^{3+} -O-Mn³⁺ ferromagnetic couplings. For LSCMO, however, only one T_C is clear, most likely due to Co^{2+} -O-Mn⁴⁺ long-range interaction. The increased T_C of LCCMO (165 K) and LSCMO (205 K) in relation to LCMO (150 K) is primarily because of structural changes in crystallinity and bond angles and lengths. No zero or even conventional exchange bias effect is seen for the Ca- and Sr-doped single crystals, in sharp contrast to polycrystalline samples [2–5]. The absence of the ZEB effect might be due to the lack of a spin-glass-like phase and/or grain boundary interfaces in these single crystals. Further studies on the spin dynamics may elucidate the nonexistence of the ZEB effect in single crystalline samples and give insights into the critical properties necessary for its appearance.

ACKNOWLEDGMENTS

This work was supported by the Brazilian funding agencies: Fundação Carlos Chagas Filho de Amparo à Pesquisa do Estado do Rio de Janeiro (FAPERJ) (Grant No. E-26/202.798/2019), Fundação de Amparo à Pesquisa do Estado de Goiás (FAPEG) and Conselho Nacional de Desenvolvimento Científico e Tecnológico (CNPq) (No. 400633/2016-7). The work at the University of Warwick was funded by the Engineering and Physical Sciences Research Council (EPSRC), United Kingdom (Grant No. EP/T005963/1).

-
- [1] S. Vasala and M. Karppinen, *Prog. Solid State Chem.* **43**, 1 (2015).
- [2] J. K. Murthy and A. Venimadhav, *Appl. Phys. Lett.* **103**, 252410 (2013).
- [3] J. K. Murthy, K. D. Chandrasekhar, H. C. Wu, H. D. Yang, J. Y. Lin, and A. Venimadhav, *J. Phys.: Condens. Matter* **28**, 086003 (2016).
- [4] R. C. Sahoo, D. Paladhi, P. Dasgupta, A. Poddar, R. Singh, A. Das, and T. K. Nath, *J. Magn. Magn. Mater.* **428**, 86 (2017).
- [5] L. T. Coutrim, D. Rigitano, C. Macchiutti, T. J. A. Mori, R. Lora-Serrano, E. Granado, E. Sadrollahi, F. J. Litterst, M. B. Fontes, E. Baggio-Saitovitch, E. M. Bittar, and L. Bufaiçal, *Phys. Rev. B* **100**, 054428 (2019).
- [6] L. T. Coutrim, E. M. Bittar, F. Stavale, F. Garcia, E. Baggio-Saitovitch, M. Abbate, R. J. O. Mossaneck, H. P. Martins, D. Tobia, P. G. Pagliuso, and L. Bufaiçal, *Phys. Rev. B* **93**, 174406 (2016).
- [7] L. Bufaiçal, R. Finkler, L. T. Coutrim, P. G. Pagliuso, C. Grossi, F. Stavale, E. Baggio-Saitovitch, and E. M. Bittar, *J. Magn. Magn. Mater.* **433**, 271 (2017).
- [8] L. Xie and H. G. Zhang, *Curr. Appl. Phys.* **18**, 261 (2018).
- [9] S. K. Giri, R. C. Sahoo, P. Dasgupta, A. Poddar, and T. K. Nath, *J. Phys. D: Appl. Phys.* **49**, 165002 (2016).

- [10] J. Nogués and I. K. Schuller, *J. Magn. Magn. Mater.* **192**, 203 (1999).
- [11] L. T. Coutrim, E. M. Bittar, F. Garcia, and L. Bufaiçal, *Phys. Rev. B* **98**, 064426 (2018).
- [12] L. Bufaiçal, L. T. Coutrim, E. M. Bittar, and F. Garcia, *J. Magn. Magn. Mater.* **512**, 167048 (2020).
- [13] V. M. Goldschmidt, *Naturwissenschaften* **14**, 477 (1926).
- [14] J. B. Goodenough, *Magnetism and Chemical Bond* (Interscience, New York, 1963).
- [15] G. Blasse, *J. Phys. Chem. Solids* **26**, 1969 (1965).
- [16] M. P. Singh, K. D. Truong, and P. Fournier, *Appl. Phys. Lett.* **91**, 042504 (2007).
- [17] Y. Q. Lin and X. M. Chen, *J. Am. Ceram. Soc.* **94**, 782 (2011).
- [18] R. I. Dass and J. B. Goodenough, *Phys. Rev. B* **67**, 014401 (2003).
- [19] C. L. Bull, D. Gleeson, and K. S. Knight, *J. Phys.: Condens. Matter* **15**, 4927 (2003).
- [20] Y. Bai, Y. Xia, H. Li, L. Han, Z. Wang, X. Wu, S. Lv, X. Liu, and J. Meng, *J. Phys. Chem. C* **116**, 16841 (2012).
- [21] M. Boldrin, A. G. Silva, L. T. Coutrim, J. R. Jesus, C. Macchiutti, E. M. Bittar, and L. Bufaiçal, *Appl. Phys. Lett.* **117**, 212402 (2020).
- [22] W.-G. Huang, X.-Q. Zhang, H.-F. Du, R.-F. Yang, Y.-K. Tang, Y. Sun, and Z.-H. Cheng, *J. Phys.: Condens. Matter* **20**, 445209 (2008).
- [23] L. Xiao, Z. Xia, Z. Jin, L. Shi, Y. Ni, J. Zhang, and W. Yu, *Ceram. Int.* **42**, 2550 (2016).
- [24] X. Wang, S. Gao, X. Yan, Q. Li, J. Zhang, Y. Long, K. Ruan, and X. Li, *Phys. Chem. Chem. Phys.* **20**, 3687 (2018).
- [25] I. Fita, A. Wisniewski, R. Puzniak, E. E. Zubov, V. Markovich, and G. Gorodetsky, *Phys. Rev. B* **98**, 094421 (2018).
- [26] S. Ding, M. Xue, Z. Liang, Z. Liu, R. Li, S. Cao, Y. Sun, J. Zhao, W. Yang, and J. Yang, *J. Phys.: Condens. Matter* **31**, 435801 (2019).
- [27] A. C. Larson and R. B. Von Dreele, Los Alamos National Laboratory Report No. LAUR 86-748, 2000 (unpublished); B. H. Toby, *J. Appl. Crystallogr.* **34**, 210 (2001).
- [28] M. Balanda, *Acta Phys. Pol., A* **124**, 964 (2013).
- [29] K. Manna, V. S. Bhadram, S. Elizabeth, C. Narayana, and P. S. A. Kumar, *J. Appl. Phys.* **116**, 043903 (2014).
- [30] H. Y. Choi, S. H. Oh, J. Y. Moon, M. K. Kim, D. G. Oh, N. Lee, and Y. J. Choi, *Phys. Status Solidi RRL* **9**, 663 (2015).
- [31] M. Balli, P. Fournier, S. Jandl, K. D. Truong, and M. M. Gospodinov, *J. Appl. Phys.* **116**, 073907 (2014).
- [32] T. Burnus, Z. Hu, H. H. Hsieh, V. L. J. Joly, P. A. Joy, M. W. Haverkort, H. Wu, A. Tanaka, H.-J. Lin, C. T. Chen, and L. H. Tjeng, *Phys. Rev. B* **77**, 125124 (2008).
- [33] J. Krishnamurthya and A. Venimadhav, *J. Magn. Magn. Mater.* **500**, 166387 (2020).
- [34] V. A. Khomchenko, I. O. Troyanchuk, A. P. Sazonov, V. V. Sikolenko, H. Szymczak, and R. Szymczak, *J. Phys.: Condens. Matter* **18**, 9541 (2006).
- [35] V. Cuartero, J. Blasco, J. García, J. A. Rodríguez-Velamazán, and C. Ritter, *EPJ Web Conf.* **40**, 15002 (2013).
- [36] R. D. Shannon, *Acta Crystallogr., Sect. A: Cryst. Phys. Diffr., Theor. Gen. Crystallogr.* **32**, 751 (1976).
- [37] Y. Tokura and Y. Tomioka, *J. Magn. Magn. Mater.* **200**, 1 (1999).
- [38] B. M. Wang, Y. Liu, P. Ren, B. Xia, K. B. Ruan, J. B. Yi, J. Ding, X. G. Li, and L. Wang, *Phys. Rev. Lett.* **106**, 077203 (2011).
- [39] T. Maity, S. Goswami, D. Bhattacharya, and S. Roy, *Phys. Rev. Lett.* **110**, 107201 (2013).
- [40] A. K. Nayak, M. Nicklas, S. Chadov, C. Shekhar, Y. Skourski, J. Winterlik, and C. Felser, *Phys. Rev. Lett.* **110**, 127204 (2013).